



# CHORUS

This is the accepted manuscript made available via CHORUS. The article has been published as:

## Kondo Interactions from Band Reconstruction in YbInCu<sub>4</sub>

I. Jarrige, A. Kotani, H. Yamaoka, N. Tsujii, K. Ishii, M. Upton, D. Casa, J. Kim, T. Gog, and  
J. N. Hancock

Phys. Rev. Lett. **114**, 126401 — Published 27 March 2015

DOI: [10.1103/PhysRevLett.114.126401](https://doi.org/10.1103/PhysRevLett.114.126401)

# Kondo interactions from band reconstruction in YbInCu<sub>4</sub>

I. Jarrige,<sup>1,\*</sup> A. Kotani,<sup>2</sup> H. Yamaoka,<sup>3</sup> N. Tsujii,<sup>4</sup> K. Ishii,<sup>5</sup>  
M. Upton,<sup>6</sup> D. Casa,<sup>6</sup> J. Kim,<sup>6</sup> T. Gog,<sup>6</sup> and J. N. Hancock<sup>7</sup>

<sup>1</sup>*Photon Sciences Directorate, Brookhaven National Laboratory, Upton, NY 11973-5000, USA*

<sup>2</sup>*Photon Factory, Institute of Materials Structure Science,*

*High Energy Accelerator Research Organization, 1-1 Oho, Tsukuba, Ibaraki 305-0801, Japan*

<sup>3</sup>*RIKEN SPring-8 Center, Sayo, Hyogo 679-5148, Japan*

<sup>4</sup>*Quantum Beam Center, National Institute for Materials Science, 1-2-1 Sengen, Tsukuba 305-0047, Japan*

<sup>5</sup>*Japan Atomic Energy Agency, SPring-8, Sayo, Hyogo 679-5148, Japan*

<sup>6</sup>*Advanced Photon Source, Argonne National Laboratory, Argonne, Illinois 60439, USA*

<sup>7</sup>*Department of Physics and Institute for Materials Science,  
University of Connecticut, Storrs, CT 06269, USA*

We combine resonant inelastic X-ray scattering (RIXS) and model calculations in the Kondo lattice compound YbInCu<sub>4</sub>, a system characterized by a dramatic increase in Kondo temperature and associated valence fluctuations below a first-order valence transition at  $T \simeq 42$  K. The bulk-sensitive, element-specific, and valence-projected charge excitation spectra reveal an unusual quasi-gap in the Yb-derived state density which drives an instability of the electronic structure and renormalizes the low-energy effective Hamiltonian at the transition. Our results provide long-sought experimental evidence for a link between temperature-driven changes in the low-energy Kondo scale and the higher-energy electronic structure of this system.

PACS numbers: 71.20.Eh, 78.70.Ck, 72.15.Qm, 75.20.Hr

The first-order isostructural valence transition in YbInCu<sub>4</sub> is one of the most intriguing localization-delocalization problems in correlated electron systems. Unlike model impurity systems and many Kondo lattice materials which are characterized by a single Kondo temperature  $T_K$ , YbInCu<sub>4</sub> undergoes a dramatic step-like increase of the Kondo coupling scale from  $T_K=25$  K to  $T_K=400$  K upon cooling below 42 K with associated changes in the Yb valence (2.96 to 2.83)<sup>1,2</sup>, pointing to an anomalous increase in screening of the local moment sublattice. While valence transitions in  $f$  electron systems can usually be explained on the basis of either of two possible theoretical approaches, the Kondo volume collapse (KVC) and the Mott transition, no such conclusive theoretical interpretation has yet been advanced for the transition in YbInCu<sub>4</sub>. The strong coupling between volume and  $T_K$  assumed in the KVC is not supported by the relatively small value reported for the appropriate Grüneisen parameter<sup>3,4</sup>, and the Mott transition scenario is ruled out by the 0.5% increase in the volume at the transition<sup>5</sup>. A different theoretical approach attributes the enhancement of the Kondo coupling at the transition to a larger exchange interaction between the  $f$  and conduction-band electron spins resulting from an increase of the Coulomb interaction<sup>6</sup>.

During the past decade, a number of spectroscopic measurements have added valuable pieces to the puzzle of the nature of the electronic phase transition. Fine measurements of the Yb valence, enabled by the emergence of advanced hard x-ray core-level spectroscopies like resonant x-ray emission spectroscopy<sup>2</sup>, hard X-ray photoelectron spectroscopy<sup>7</sup>, and X-ray absorption spectroscopy (XAS) in the partial fluorescence yield mode<sup>8</sup> highlight the sensitivity of X-ray probes to the valence

transition in this system. Meanwhile, using softer photons, optical conductivity measurements revealed a mid-infrared peak associated with the Kondo resonance below  $T_K$ <sup>9-12</sup>, which appears to be a universal trait of Kondo lattice and heavy fermion systems. On the other hand, while detailed knowledge of the electronic structure is essential to understanding valence transitions<sup>13,14</sup>, the high electronic dimensionality and known surface sensitivity in mixed valence systems limit the effectiveness of traditional approaches<sup>2,12,15,16</sup> to probing the electronic structure of YbInCu<sub>4</sub>.

In order to fill this gap in our understanding, we used RIXS, a bulk-sensitive, orbital and element-selective probe of the electronic structure to explore the changes in low-energy states while crossing the valence transition. RIXS is a Raman process which generates low-lying excitations through resonant X-ray edge intermediate states of well-defined orbital character. In our measurements at the Yb- $L_3$  edge, a  $2p$  core electron is photoexcited into a valence state of  $d$  character, followed by decay of a  $d$ -character valence electron into the core hole<sup>17</sup>. The nascent presence of the  $2p$  core hole potential induces excitations among rare-earth  $5d$  states, which are forbidden through direct dipole transitions relevant to optical conductivity. Here we observe several intense RIXS-active excitations, and use the valence selectivity of RIXS to uncover temperature-driven spectral changes up to several eV. These changes trend with an energy shift of itinerant  $5d$  states, revealing the energetics of an underlying instability driving the transition.

Our experiments were performed at the MERIX endstation of the XOR-IXS 30-ID beamline at the Advanced Photon Source<sup>18</sup>. Single crystals of YbInCu<sub>4</sub> were grown using the flux method and cleaved<sup>12</sup> before measurement

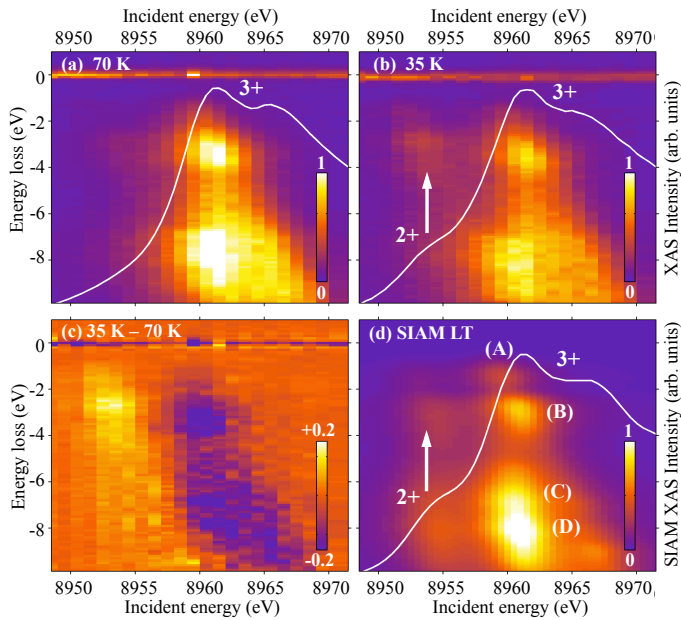


FIG. 1. (Color online) Color plot of the Yb- $L_3$  RIXS plane with the absorption spectrum (solid white line) measured at (a) 70 K and (b) 35 K, and (d) calculated for the LT phase using the SIAM and scaled to the experimental intensity. (c) The difference between the spectra measured at 35 K and 70 K. The excitation labels (A), (B), (C), (D) correspond to the transitions in Fig. 2(a).

with crystal facet along (111). YbInCu<sub>4</sub> has the cubic C15b (AuBe<sub>5</sub> type) structure<sup>19</sup>. The horizontally polarized incident beam was monochromatized using a four-bounce scheme of asymmetrically cut Si(400) crystals, scattered from the sample, and energy analyzed with a 4" diameter diced Ge (008) spherical analyzer and a strip detector placed on a 1-m Rowland spectrometer. A resultant energy resolution of 0.2 eV was achieved in the horizontal scattering geometry, with a scattering angle of 90° and momentum transfer  $Q=(5.5,3.5,3.5)$  indexed to the cubic unit cell, which contains 4 formula units.

Figs. 1(a) and 1(b) show the XAS spectra as a white curve superimposed over the Yb  $L_3$  RIXS planes for the high-temperature (HT, 70 K) and low-temperature (LT, 35 K) phases, respectively. The HT XAS spectrum displays prominent structures at 8961 eV and 8965 eV, which represent core-hole containing final states (RIXS intermediate states) with mainly  $4f^{13}$  electron configuration (Yb<sup>3+</sup>)<sup>20,21</sup>. In the LT phase, an additional shoulder emerges at a lower energy of 8953 eV and contains mainly  $4f^{14}$  character (Yb<sup>2+</sup>). The strong core hole potential is responsible for the reversal of energy ordering of these valence configurations relative to the lower energy (<10 eV) manifold. The excited core hole has many possible decay channels, one of which is the spectrally-resolved RIXS process. As indicated by the arrow in Fig. 1(b), a RIXS-active excitation around 3 eV strengthens when the incident energy is tuned near the Yb<sup>2+</sup> feature in

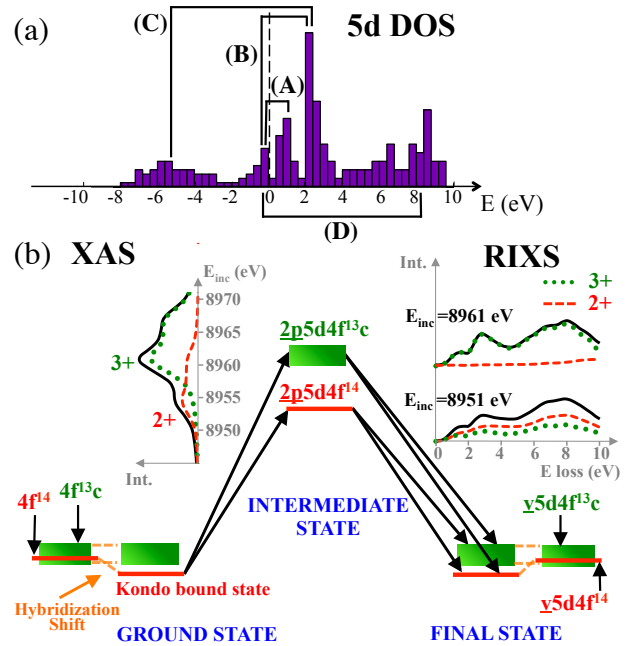


FIG. 2. (Color online) (a) Band diagram showing the occupied and unoccupied Yb  $d$  DOS used in the SIAM and the transitions assigned to RIXS peaks. (b) Total energy level scheme for a mixed-valence Yb ion, with radiative transitions in the SIAM and calculated RIXS and XAS spectral functions and their Yb<sup>2+</sup> and Yb<sup>3+</sup> components.

the LT phase. Figure 1(c) displays the intensity difference between the LT and HT RIXS planes of Figs. 1(b) and 1(a), highlighting additional changes in the <10 eV range, and revealing that scattering through the Yb<sup>3+</sup> and Yb<sup>2+</sup> resonances evolves in opposite ways across the valence transition.

To better understand the nature of the observed spectra, the incident energy dependent RIXS spectrum was calculated using the single-impurity Anderson model (SIAM)<sup>21–23</sup> and is shown for the LT phase in Figure 1(d). The remarkable agreement with the experimental data of Fig. 1(b) was achieved using a detailed bare band structure of the Yb  $d$  density of states (DOS)<sup>20</sup> which was calculated within the local-spin density approximation and includes on-site  $4f$  Coulomb interaction (LSDA+U), and is reproduced as a histogram in Fig. 2(a). Fig. 2(b) depicts the radiative transitions for the XAS and RIXS processes in the many-body SIAM<sup>21</sup>. The green rectangles represent the unoccupied part of the ligand band corresponding to the continuum of transitions between the multi-electronic  $4f^{14}$  and  $4f^{13}c$  levels, where  $c$  is an electron transferred to the ligand band. The RIXS intermediate and final state configurations respectively have a hole in the  $2p$  level and in the  $5d$  valence band, and there are four transition paths allowed<sup>24</sup>. The calculated RIXS spectral functions in Fig. 2(b) explicitly illustrate the tunable valence state selectivity through the incident energy dependence of the RIXS cross section. The SIAM

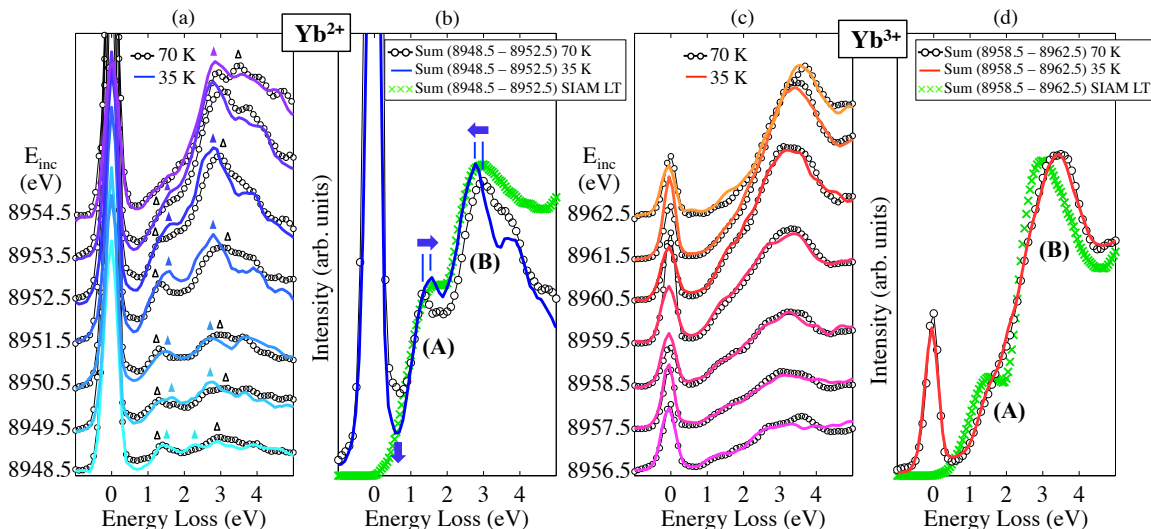


FIG. 3. (Color online) Incident energy resolved RIXS profile measured at 35 K and 70 K across the 8948.5 - 8952.5 eV (a) and 8958.5 to 8962.5 eV (c) incident energy ranges, which respectively correspond to the  $\text{Yb}^{2+}$  and  $\text{Yb}^{3+}$  components in the LT XAS spectrum. In (a), the filled and open triangles indicate the peak position of (A) and (B) at 35 and 70 K, respectively. The  $\text{Yb}^{3+}$  spectra in (c) are intensity scaled by 0.4 for comparison with  $\text{Yb}^{2+}$  in (a), and for each incident energy the HT spectra are normalized to the area of the LT spectra over the 0.5-5.0 eV range to ease the comparison between the low-energy features. The raw RIXS spectra averaged over these respective incident energy ranges are shown in (b) and (d) along with the corresponding calculated spectra for the LT phase. In (b), the arrows indicate the direction of variations in the RIXS intensity upon cooling from 70 to 35 K.

is explained in more detail in Ref. 25.

The agreement between the panels Fig. 1(b) and (d) permits assignment of the salient spectral features to specific electronic transitions among Yb 5d occupied and unoccupied states (see Fig. 2(a)). The RIXS process responsible for the small structure labeled (A) at  $\sim 1.5$  eV involves photoexcitation of a core electron into the shoulder of the unoccupied 5d DOS around 1.5 eV above the Fermi level  $E_F$ , followed by coherent recombination of an electron from the 5d peak just below  $E_F$  into the core hole. A second, stronger feature centered around 3 eV, and two higher-energy excitations in the 6-10 eV range correspond respectively to the transitions signified by the lines labeled (B), (C) and (D) in Fig. 2(a).

We now show that the valence-selective nature of the RIXS probe provides unique insight into the dependence of the low-energy charge excitations on the  $f$  shell occupancy. Figs. 3(a) and 3(c) respectively show the incident-energy resolved RIXS spectra separately for the energy ranges corresponding to the  $\text{Yb}^{2+}$  (8948.5 - 8952.5 eV) and  $\text{Yb}^{3+}$  (8958.5 - 8962.5 eV) components in the LT XAS spectrum. To simplify presentation, these RIXS spectra were averaged over the energy windows around each intermediate valence state and are shown in Fig. 3(b) and 3(d) respectively, along with the corresponding SIAM summed intensity for the LT phase. Upon cooling across the transition, the spectra for the  $\text{Yb}^{3+}$  intermediate states show only weak changes, while those for the  $\text{Yb}^{2+}$  intermediate states reveal dramatic reconstruction, with a quasigap-like dip opening around 0.5 eV, and the

shifts of the features (A) and (B) by respectively +0.2 and -0.2 eV.

The RIXS-enabled selectivity of excitations related to the divalent state reveals an unprecedentedly clear view of the temperature-induced changes in Yb 5d states. In the LT phase, the Yb mean valence drops to 2.83 and an XAS shoulder related to  $\text{Yb}^{2+}$  appears (see Fig. 1(b)). An attempt to understand the dependence of charge excitations on  $f$  occupancy was made in the context of optical spectra<sup>20</sup>, where calculations within the LSDA+U and LSDA approximations yielded  $f$  counts of nearly 13 ( $\text{Yb}^{3+}$ ) and 14 ( $\text{Yb}^{2+}$ ), respectively, and a virtual crystal variant of the LSDA+U covered intermediate valence cases of  $\text{Yb}^{2.8+}$  and  $\text{Yb}^{2.9+}$ . For the increased  $f$  count, mimicking the LT phase, more effective screening of the Yb nuclear charge was found to cause a shift of the empty on-site Yb 5d band upwards towards lower binding energies, while off-site electronic states derived from high binding energy In 5p states are less sensitive to changes in screening efficiency. This effect was suggested to explain valence transition-induced shift observed in a set of In 5p  $\rightarrow$  Yb 5d interband transitions which strongly resemble feature (A) in our RIXS spectra. The similar absolute energy, magnitude, and sign of the shift of the optical transitions and feature (A) suggests that the nuclear screening effect is also manifest in the Yb 5d  $\rightarrow$  Yb 5d RIXS interband transitions.

Feature (B) was not observed in optical conductivity and is *redshifted* by 0.2 eV in the LT-RIXS spectrum. The opposite temperature-dependent behavior of the fea-

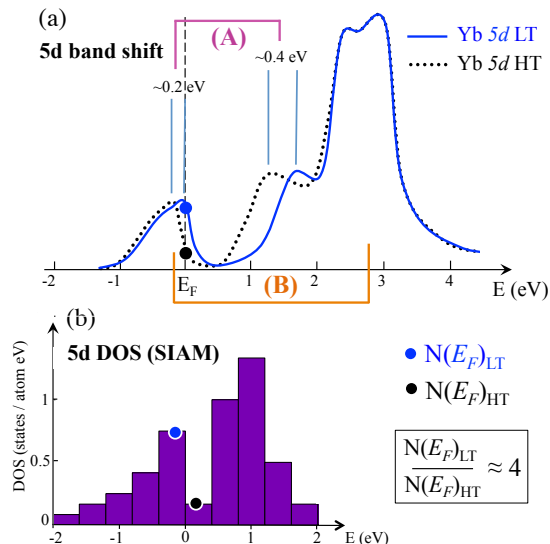


FIG. 4. (Color online) (a) Schematic illustration of the non-rigid shift of the Yb 5d band across the transition. The shift towards lower binding energies is about twice for the shoulder in the unoccupied states around 1.5 eV than for the occupied states, as inferred from the 0.2 eV blueshift of (A) and 0.2 eV redshift of (B) in the RIXS data. (b) The Fermi level moves out of the quasigap while the Yb 5d Fermi DOS (Fig. 2(a)) sharply increases at LT.

tures (A) and (B) coupled with our convincing assignment of these features within the LT phase shown in Figs. 1b and 1d implies that a rigid-shift picture of the Yb 5d band breaks down across the transition. While further theoretical treatment is appropriate to better understand the detailed cause-effect connections between nuclear screening,  $f$  count, and the observed electronic structure changes, here we explore possible influences on the non-rigid 5d band, as schematically illustrated in Fig. 4(a). Optical conductivity measurements have revealed a sharp mid-infrared peak associated with Kondo resonance formation below  $T_K$ <sup>10-12</sup>, ascribed to dipole-active transitions across the correlation-induced gap between hybridized bands near  $E_F$ . We speculate that the formation of these hybridized bands may play a role in partially pinning the 5d states located around  $E_F$  due to the more effective mixing with the 4f-hybridizing In 5p states at higher binding energy, and that the portion of the unoccupied 5d band at lower binding energy is less sensitive to changes in screening efficiency. While the detailed origin of these marked spectral changes requires advanced theoretical methods such as dynamical mean field theory, our experimental exploration of the partial DOS enabled by RIXS gives a new window into the electronic structure of this and other strongly correlated electron systems.

We now turn to the quasigap observed around 0.5 eV in Fig. 3(b), and its relation with the quasigap in the DOS around  $E_F$ <sup>20,27</sup>. As illustrated in Fig. 4(a), the shift of the Yb 5d occupied and unoccupied bands towards lower binding energies is expected to push the quasigap away

from the Fermi level. To estimate the effect on parameters relevant to the macroscopic material behavior, we use the observed shift  $\sim 0.2$  eV and calculated Yb 5d DOS to estimate  $N(E_F)_{LT}/N(E_F)_{HT} \approx 4$  as a rough fractional change in 5d Fermi DOS upon cooling through the transition (see Fig. 4(b)). This is consistent with the jump in the carrier concentration observed below the transition<sup>5</sup> and the observed lowering of RIXS intensity in this spectral region, and would cause the abrupt rise of  $T_K$  at LT, as discussed below. A link between a subtle change in the position of the DOS quasigap with respect to  $E_F$  and the transition had been previously hypothesized on the basis of Hall effect<sup>28</sup> and Cu-2p<sub>3/2</sub> XAS spectra<sup>29</sup>, and our results provide direct evidence for this relationship.

Within the SIAM,  $T_K$  can be expressed as  $k_B T_K = [(1 - n_h)/n_h] N_f \tilde{V}^2$ , where  $\tilde{V}^2 = \rho(E_F) V^2$ ,  $n_h$  is the number of 4f holes and  $N_f$  is the degeneracy of the 4f states.  $\rho(E_F)$  is the partial DOS of the relevant ligand band, which is primarily derived from extended In 5p orbitals. Yb 5d and In 5p bands have dominant contributions to the carrier concentration and are expected to be strongly hybridized with each other due to their large orbital extent and close physical proximity, a fact supported by the similarities between these partial DOS in energy band calculations<sup>20,27</sup>. To estimate the DOS effect on  $T_K$ , we assume that the strong correlation between the Yb 5d DOS  $N(E_F)$  and ligand DOS  $\rho(E_F)$  is such that a variation in  $N(E_F)$  gives rise to a proportional variation in  $\rho(E_F)$ . Under this assumption, the ratio  $\rho(E_F)_{LT}/\rho(E_F)_{HT}$  is approximately the same as  $N(E_F)_{LT}/N(E_F)_{HT}$ ,  $\sim 4$ . In fact, using the experimentally derived values of  $n_h$  and  $T_K$ <sup>1,2</sup> in the above expression of  $T_K$ , one estimates  $(V^2 \rho(E_F))_{LT}/(V^2 \rho(E_F))_{HT} = 3.2$ , which is reasonably close to our estimation of  $\rho(E_F)_{LT}/\rho(E_F)_{HT}$ , suggesting that the first-order change in  $T_K$  is largely due to the jump in DOS at  $E_F$ , in stark contrast to the phenomenologically similar  $\gamma$ - $\alpha$  transition in Ce, which is usually interpreted in terms of a volume-induced change of  $V$ <sup>30</sup>. We also note that related systems YbInCu<sub>5</sub><sup>31</sup> and YbAgCu<sub>4</sub><sup>5</sup> show continuous valence crossover behavior, and have relatively smooth and quasigap-free near- $E_F$  DOS profiles, bolstering the key role of the strongly indented profile of the DOS around  $E_F$  in the anomalous first-order transition in YbInCu<sub>4</sub>.

We have carried out RIXS measurements of YbInCu<sub>4</sub> across the isostructural valence transition, which show pronounced electronic structure changes, particularly for excitations derived from divalent intermediate states. These changes indicate that the Fermi level migrates out of an unusual quasigap following the onset of the mixed-valence behavior at LT. The striking rise of  $T_K$  below the transition is a result of sharp contrast in the energy-dependent state density near the Fermi level, a condition which is left out of common theoretical considerations of the Kondo effect. These results establish a link between the bare band structure and the Kondo scale at the heart of the valence transition. Through a novel application

of RIXS, we have clearly demonstrated how the valence sensitivity of this emerging spectroscopic technique can disclose subtle changes in electronic structure to reveal new physics in the context of Kondo interactions.

## ACKNOWLEDGMENTS

We thank T. Fukuda for his help with aligning the single crystal.

- 
- \* To whom correspondence should be addressed: E-mail: jarrige@bnl.gov
- <sup>1</sup> J. L. Sarrao, C. D. Immer, C. L. Benton, Z. Fisk, J. M. Lawrence, D. Mandrus and J. D. Thompson, Phys. Rev. B **54**, 12207 (1996).
  - <sup>2</sup> C. Dallera, M. Grioni, A. Shukla, G. Vankó, J.L. Sarrao, J.P. Rueff, and D.L. Cox, Phys. Rev. Lett. **88**, 196403-1 (2002).
  - <sup>3</sup> A Yu Sokolov, H Nakamura, and M Shiga, J. Phys.: Condens. Matter **11**, 6463 (1999).
  - <sup>4</sup> J. L. Sarrao, A. P. Ramirez, T. W. Darling, F. Freibert, A. Migliori, C. D. Immer, Z. Fisk, and Y. Uwatoko, Phys. Rev. B **58**, 409 (1998).
  - <sup>5</sup> A. L. Cornelius, J. M. Lawrence, J. L. Sarrao, Z. Fisk, M. F. Hundley, G. H. Kwei, J. D. Thompson, C. H. Booth, and F. Bridges, Phys. Rev. B **56**, 7993 (1997).
  - <sup>6</sup> A.V. Goltsev and G. Bruls, Phys. Rev. B **63**, 155109 (2001).
  - <sup>7</sup> H. Sato, K. Shimada, M. Arita, K. Hiraoka, K. Kojima, Y. Takeda, K. Yoshikawa, M. Sawada, M. Nakatake, H. Namatame, M. Taniguchi, Y. Takata, E. Ikenaga, S. Shin, K. Kobayashi, K. Tamasaku, Y. Nishino, D. Miwa, M. Yabashi, and T. Ishikawa, Phys. Rev. Lett. **93**, 246404 (2004).
  - <sup>8</sup> H. Yamaoka, N. Tsujii, K. Yamamoto, A. M. Vlaicu, H. Ohashi, H. Yoshikawa, T. Tochio, Y. Ito, A. Chainani, and S. Shin, Phys. Rev. B **78**, 045127 (2008).
  - <sup>9</sup> S.R. Garner, J. N. Hancock, Y.W. Rodriguez, Z. Schlesinger, B. Bucher, Z. Fisk, and J.L. Sarrao, Phys. Rev. B **62**, 4778(R) (2000).
  - <sup>10</sup> J. N. Hancock, T. McKnew, Z. Schlesinger, J. L. Sarrao, and Z. Fisk, Phys. Rev. Lett. **92**, 186405 (2004).
  - <sup>11</sup> J. N. Hancock, T. McKnew, Z. Schlesinger, J. L. Sarrao, and Z. Fisk, Phys. Rev. B **73**, 125119 (2006).
  - <sup>12</sup> H. Okamura, T. Michizawa, T. Nanba, and T. Ebihara, Phys. Rev. B **75**, 041101(R) (2007).
  - <sup>13</sup> P. Strange, A. Svane, W. M. Temmerman, Z. Szotek, and H. Winter, Nature (London) **399**, 756 (1999).
  - <sup>14</sup> W. M. Temmerman, A. Svane, L. Petit, M. Luders, P. Strange, and Z. Szotek, Phase Transit. **80**, 415 (2007).
  - <sup>15</sup> F. Reinert, R. Claessen, G. Nicolay, D. Ehm, S. Hüfner, W.P. Ellis, G.-H. Gweon, J.W. Allen, B. Kindler, and W. Assmus, Phys. Rev. B **58**, 12808 (1998).
  - <sup>16</sup> D.P. Moore, J.J. Joyce, A.J. Arko, J.L. Sarrao, L. Morales, H. Hochst, and Y.D. Chuang, Phys. Rev. B **62**, 16492 (2000).
  - <sup>17</sup> A. Kotani, K.O. Kvashnina, S.M. Butorin, and P. Glatzel, Eur. Phys. J. B **85**, 257 (2012).
  - <sup>18</sup> Y. Shvyd'ko, J. Hill, C. Burns, D. Coburn, B. Brajuskovic, D. Casa, K. Goetze, T. Gog, R. Khachatryan, J.-H. Kim, C. Kodituwakku, M. Ramanathan, T. Roberts, A. Said, H. Sinn, D. Shu, S. Stoupin, M. Upton, M. Wiczorek, and H. Yavas, J. Electron Spectrosc. Related Phenom. **188**, 140 (2013).
  - <sup>19</sup> J.M. Lawrence, G.H. Kwei, J.L. Sarrao, Z. Fisk, D. Mandrus, and J.D. Thompson, Phys. Rev. B **54**, 6011 (1996).
  - <sup>20</sup> V. N. Antonov, M. Galli, F. Marabelli, A. N. Yaresko, A. Ya. Perlov, and E. Bauer, Phys. Rev. B **62**, 1742 (2000).
  - <sup>21</sup> A. Kotani, Eur. Phys. J. B **85**, 31 (2012).
  - <sup>22</sup> A. Kotani, K. O. Kvashnina, P. Glatzel, J. C. Parlebas and G. Schmerber, Phys. Rev. Lett. **108**, 036403 (2012).
  - <sup>23</sup> A. Kotani, Mod. Phys. Letters B **27**, 1330012 (2013).
  - <sup>24</sup> We note that the model is set to simulate the so-called direct RIXS process as described in ref. 17, which consists of an excitation from the core level  $2p$  to an empty  $5d$  state in the intermediate state followed by the filling of the  $2p$  core hole by an electron from an occupied  $5d$  state in the final state. The so-called indirect RIXS process, which occurs via a shake-up of the electronic system in presence of the core hole, is forbidden for a scattering angle of  $90^\circ$ <sup>17</sup>, which we used in the experiment, and is therefore not included in the model.
  - <sup>25</sup> See Supplemental Material, which includes Ref. 26.
  - <sup>26</sup> O. Gunnarsson and K. Schönhammer, Phys. Rev. B **28**, 4315 (1983).
  - <sup>27</sup> K. Takehagara and T. Kasuya, J. Phys. Soc. Jpn. **59**, 3299 (1990).
  - <sup>28</sup> E. Figueroa, J.M. Lawrence, J.L. Sarrao, Z. Fisk, M.F. Hundley, and J.D. Thompson, Solid State Comm. **106**, 347 (1998).
  - <sup>29</sup> Y. Utsumi, H. Sato, H. Kurihara, H. Maso, K. Hiraoka, K. Kojima, K. Tobimatsu, T. Ohkochi, S.-i. Fujimori, Y. Takeda, Y. Saitoh, K. Mimura, S. Ueda, Y. Yamashita, H. Yoshikawa, K. Kobayashi, T. Oguchi, K. Shimada, H. Namatame, and M. Taniguchi, Phys. Rev. B **84**, 115143 (2011).
  - <sup>30</sup> See for instance K. Haule, V. Oudovenko, S.Y. Savrasov, and G. Kotliar, Phys. Rev. Lett. **94**, 036401-1 (2005).
  - <sup>31</sup> H. Yamaoka, I. Jarrige, N. Tsujii, N. Hiraoka, H. Ishii, and K.-D. Tsuei, Phys. Rev. B **80**, 035120 (2009).